
MapPFN: Learning Causal Perturbation Maps in Context

Marvin Sextro^{1,2,3} Weronika Kłós^{1,2} Gabriel Dernbach^{1,4,2,3}

Abstract

Planning effective interventions in biological systems requires treatment-effect models that adapt to unseen biological contexts by identifying their specific underlying mechanisms. Yet single-cell perturbation datasets span only a handful of biological contexts, and existing methods cannot leverage new interventional evidence at inference time to adapt beyond their training data. To meta-learn a perturbation effect estimator, we present MapPFN, a prior-data fitted network (PFN) pre-trained on synthetic data generated from a prior over causal perturbations. Given a set of experiments, MapPFN uses in-context learning to predict post-perturbation distributions. Pre-trained on *in silico* gene knockouts alone, MapPFN identifies differentially expressed genes on par with models trained on real single-cell data. Fine-tuned, it consistently outperforms baselines across downstream datasets. Our code, model and data are available at <https://marvinsxtr.github.io/MapPFN>.

1. Introduction

To gain a mechanistic understanding of the behavior of cell populations, single-cell perturbation data has long been the experimental gold standard to identify the causal dependencies that form underlying gene regulatory networks (GRNs) (Sachs et al., 2005). Genetic CRISPR knockout perturbations (Jinek et al., 2012) measured in single cells using Perturb-Seq (Dixit et al., 2016) allow us to measure the outcome of targeted interventions in controlled biological contexts like cell lines (Frangieh et al., 2021; Papalexi et al., 2021). Yet, mapping the whole space of possible cell states and perturbations through experiments alone is infeasible.

¹Machine Learning Group, Technische Universität Berlin, Berlin, Germany ²Berlin Institute for the Foundations of Learning and Data (BIFOLD) ³Agnostics, Berlin, Germany ⁴Institute of Pathology, Charité - Universitätsmedizin Berlin, Berlin, Germany. Correspondence to: Marvin Sextro <m.kleine.sextro@tu-berlin.de>.

Preprint.

This bottleneck has motivated methods that learn how cells respond to perturbations induced by small molecules or gene knockouts (Bunne et al., 2024; Roohani et al., 2025). Such virtual cell models are aimed at reducing the costs of drug target discovery, as they enable low latency and high throughput evaluation of hypotheses prior to costly and time-consuming validation in the wet lab.

Because sequencing destroys individual cells, perturbation prediction becomes a problem of mapping between unpaired distributions, making optimal transport (OT) a natural approach. These methods learn a transport map between the pre- and post-perturbation cell distributions, conditioned on a treatment or covariates (Bunne et al., 2023; Dong et al., 2023). Lifting the strict assumptions of OT-based methods, recent approaches use generative models to predict the post-perturbation distribution conditioned on covariates (Lotfolahi et al., 2023; Klein et al., 2025) or a learned representation of the initial observational distribution (Atanackovic et al., 2025; Adduri et al., 2025). Yet, they lack test-time, context-based adaptation from a small set of observed interventions, constraining generalization to the biological contexts seen during training.

In this work, we propose to meta-learn perturbation maps from a context of observational and interventional distributions, enabling a diffusion transformer to infer perturbation effects via in-context learning. Building on the recent success of prior-data fitted networks (PFNs; Müller et al., 2022) in tabular prediction (Hollmann et al., 2025; 2023; Qu et al., 2025) and causal inference (Robertson et al., 2025; Balazadeh et al., 2025; Ma et al., 2025), we introduce PFNs for perturbation prediction with a multi-experiment input to achieve foundational perturbation model pre-training on synthetic data. Different to standard PFN training, our task requires the prediction of a distribution of vectors, for which we adopt the Multimodal Diffusion Transformer (MMDiT; Esser et al., 2024) architecture. We show that conditioning on pre- and multiple post-perturbation distributions improves performance over models that only use a pre-perturbation distribution with a query treatment identifier. Pre-trained exclusively on synthetic data, MapPFN recovers differentially expressed genes, performing on par with methods trained on real single-cell data. Fine-tuned, it consistently outperforms baselines across perturbation datasets (Frangieh et al., 2021; Papalexi et al., 2021).

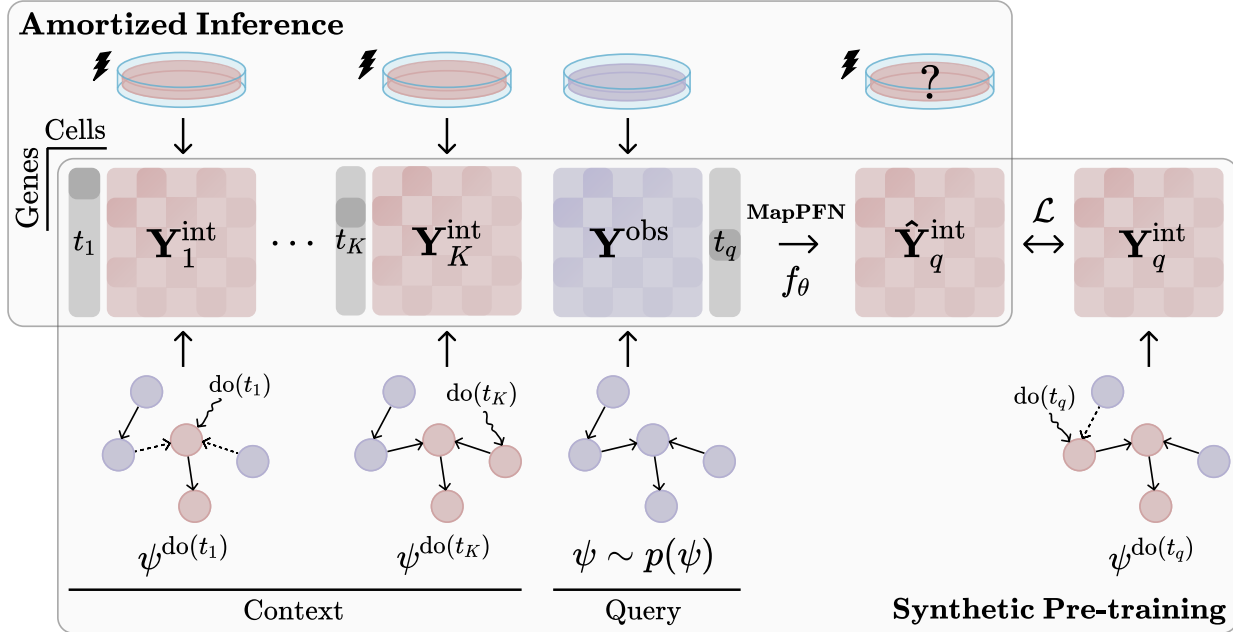


Figure 1. MapPFN overview. MapPFN uses in-context learning (ICL) to predict perturbation effects in unseen biological contexts. During pre-training, we draw structural causal models (SCMs) or synthetic gene regulatory networks (GRNs) ψ to generate samples from the observational distribution \mathbf{Y}^{obs} and a context set of interventional distributions $\mathcal{C} = \{(t_k, \mathbf{Y}_k^{\text{int}})\}_{k=1}^K$, where t_k denotes a perturbation (do-intervention). Given \mathbf{Y}^{obs} and the context set \mathcal{C} , MapPFN predicts post-perturbation distributions $\mathbf{Y}_q^{\text{int}}$ arising from unseen interventions t_q . During pre-training, MapPFN meta-learns how to map between pre- and post-perturbation distributions across many causal structures ψ by minimizing $\mathcal{L}(\hat{\mathbf{Y}}_q^{\text{int}}, \mathbf{Y}_q^{\text{int}})$. At inference time, MapPFN predicts cell-level post-perturbation distributions $\mathbf{Y}_q^{\text{int}} \in \mathbb{R}^{\text{cells} \times \text{genes}}$ in one step through amortized inference, without requiring knowledge of the underlying causal structure ψ .

Our Contributions

1. We frame perturbation prediction as a distribution mapping with test-time interventional context, enabling a single pre-trained model to adapt to unseen biological contexts and to arbitrary gene sets via in-context learning.
2. We introduce MapPFN, the first prior-data fitted network (PFN) for perturbation prediction. Pre-trained on a synthetic biological prior of *in silico* gene knockouts, MapPFN meta-learns perturbation maps across diverse causal structures and is not limited by the availability of experimental perturbation data.
3. In a controlled synthetic benchmark of structural causal models (SCMs), MapPFN outperforms existing baselines across metrics. Our ablations show that interventional context and a counterfactual prior each independently improve predictions.
4. Evaluated on biologically distinct perturbation datasets, MapPFN achieves zero-shot recovery of differentially expressed genes on par with baselines trained from scratch on real data. Fine-tuned, it consistently outperforms baselines across datasets.

2. Problem Statement

We consider the problem of learning how biological systems behave under interventions. In the case of single-cell perturbations, we are given a set of N gene expressions $\mathbf{y}^{\text{obs}} \in \mathbb{R}^d$ measured in a specific cell line and a treatment $t \in \mathcal{T}$ in the form of an intervention on a single gene, resulting in M post-treatment gene expressions $\mathbf{y}^{\text{int}} \in \mathbb{R}^d$. The resulting dataset takes the form $\{(\mathbf{Y}_\ell^{\text{obs}}, t_\ell, \mathbf{Y}_\ell^{\text{int}})\}_{\ell=1}^L$, where $\mathbf{Y}^{\text{obs}} \in \mathbb{R}^{N \times d}$, $\mathbf{Y}^{\text{int}} \in \mathbb{R}^{M \times d}$ and L is the number of pairs of biological contexts and treatments. Importantly, there is no direct correspondence between any two pre- and post-treatment cells, rendering this a problem of learning a map between distributions $p(\mathbf{y}^{\text{obs}})$ and $p(\mathbf{y}^{\text{int}})$.

The same intervention can produce different perturbation responses depending on the biological context and its underlying causal mechanisms. We therefore condition on observational samples \mathbf{Y}^{obs} and an interventional context $\mathcal{C} = \{(t_k, \mathbf{Y}_k^{\text{int}})\}_{k=1}^K$ for a subset of treatment conditions $t_k \in \mathcal{T}_{\mathcal{C}} \subset \mathcal{T}$ for a given biological context, and aim to predict the outcome distribution of an unseen query perturbation $t_q \in \mathcal{T} \setminus \mathcal{T}_{\mathcal{C}}$:

$$p(\mathbf{y}_q^{\text{int}} \mid \text{do}(t_q), \mathbf{Y}^{\text{obs}}, \mathcal{C}) \quad (1)$$

3. Related Work

Perturbation Prediction Existing methods differ in their generalization target and conditioning capabilities. Approaches like CPA (Lotfollahi et al., 2023), CellOT (Bunne et al., 2023) and CellFlow (Klein et al., 2025) condition on covariates and aim to generalize across biological contexts. Meta Flow Matching (Atanackovic et al., 2025) and STATE (Adduri et al., 2025) additionally condition on the observational distribution. Methods targeting unseen perturbations instead make assumptions about the causal structure, either through explicit modeling (Schneider et al., 2025) or by incorporating known GRNs (Roohani et al., 2024). Single-cell foundation models (Theodoris et al., 2023; Cui et al., 2024; Hao et al., 2024) perform perturbation effect analysis on individual cells rather than generating post-perturbation distributions. Our work targets generalization to unseen biological contexts and uniquely conditions on interventional data at inference time.

Amortized and In-Context Learning Rather than optimizing per task, amortized methods learn to perform inference in a single forward pass conditioned on a task context. This context can take the form of the whole dataset for causal structure learning (Lorch et al., 2022; Ke et al., 2023; Dhir et al., 2025) or an input distribution for OT (Amos et al., 2023; Klein et al., 2024) or generative modeling (Atanackovic et al., 2025). Exemplified by large language models (Brown et al., 2020), in-context learning (ICL) achieves amortization by conditioning on example tasks in the input sequence. Recent evidence shows that next-token prediction alone can induce causal discovery and counterfactual reasoning in transformers (Butkus & Kriegeskorte, 2025). Concurrent to our work, Dong et al. (2026) apply ICL to single-cell perturbation prediction. Unlike our approach, they limit the interventional context set to a single experiment and do not use a synthetic prior for pre-training.

Prior-data Fitted Networks Prior-data fitted networks (PFNs) are pre-trained on synthetic datasets to perform Bayesian inference in context (Müller et al., 2022). The datasets are generated from a pre-defined generative process, also referred to as the prior. PFNs have recently surpassed classical methods in tabular prediction benchmarks (Hollmann et al., 2025) and have been applied to other problems, including causal inference (Balazadeh et al., 2025; Robertson et al., 2025; Ma et al., 2025), full Bayesian inference (Reuter et al., 2025) and optimization (Müller et al., 2023). Yet, contrary to our approach, existing PFNs for causal inference only predict univariate outcomes for individual samples rather than population-level distributions, rendering them incapable of handling perturbation data. In addition, they focus on learning from observational data alone and do not condition predictions on interventional data.

4. Methods

Primer on Prior-data Fitted Networks In a classical supervised machine learning setting with a dataset $\mathcal{D} = \{(\mathbf{x}_i, y_i)\}_{i=1}^N$, Bayesian inference assumes a prior $p(\psi)$ representing a space of hypotheses (e.g. structural causal models) that could have generated the data. The aim of PFNs is to approximate the posterior predictive distribution (PPD) $p(y | \mathbf{x}, \mathcal{D})$. Given a complete training dataset $\mathcal{D} = \{(\mathbf{x}_i, y_i)\}_{i=1}^N$ and an unlabeled query \mathbf{x}_q from the test set, a PFN directly outputs the predicted label y_q . Since the learning process happens in the context of a transformer within a single forward pass, this process is regarded as in-context learning or amortized Bayesian inference. Training PFNs involves sampling a large number of hypotheses $\psi \sim p(\psi)$ and generating synthetic datasets $\mathcal{D} \sim p(\mathcal{D} | \psi)$ in an outer loop to meta-learn how to make predictions in context. We refer to Müller et al. (2022) and Hollmann et al. (2023) for further details.

Structural Causal Models To study perturbation prediction in a controlled environment, we set up a synthetic experiment where the true data-generating process is known. A structural causal model (SCM) ψ (Pearl, 2009) defines a generative model through a directed acyclic graph (DAG) \mathcal{G}_ψ over variables $\{z_1, z_2, \dots, z_d\}$, together with structural assignment $z_k = f_k(z_{\text{PA}(k)}, \epsilon_k)$ for each node z_k , where $z_{\text{PA}(k)}$ denotes the parents of z_k in \mathcal{G}_ψ , f_k is a deterministic function, and ϵ_k is an exogenous noise variable. Following the rules of do-calculus (Pearl, 2009), a hard intervention $\text{do}(t)$ on node z_k removes its incoming edges and assigns $z_k := t$, yielding $\psi^{\text{do}(t)}$. Specifically, we consider linear additive noise models (ANMs); a class of SCMs with linear functional relationships f_k and additive noise. In this case, the model is fully determined by a sparse weighted adjacency matrix $\mathbf{W} \in \mathbb{R}^{d \times d}$, where $w_{kj} \neq 0$ only if $j \in \text{PA}(k)$. Given a noise vector $\epsilon \sim \mathcal{N}(0, \mathbf{I})$, we can sample from linear ANMs by solving the linear system $\mathbf{z} = (\mathbf{I} - \mathbf{W})^{-1} \epsilon$ (Pearl, 2009).

Transductive Perturbation Prediction In practice, the true underlying causal structure of a given biological context is unknown and only partially identifiable from finite data. Inspired by the principle of *transduction* (Vapnik, 2006), we directly predict the post-perturbation distribution given observational and interventional data, rather than recovering the causal model as an intermediate step.

Synthetic Biological Prior Experimental perturbation screens are costly and span few biological contexts, with even the largest dataset to date covering only 50 cell lines (Zhang et al., 2025). We decouple MapPFN from this bottleneck by pre-training on synthetic datasets generated from a prior distribution over ψ , constructed from established

components validated against single-cell screens (Dibaeinia & Sinha, 2020; Aguirre et al., 2025). We sample diverse gene regulatory networks (GRN) with realistic sparsity and modular structure, from which we simulate observational and interventional gene expression dynamics. Additional details on the prior are provided in subsection 5.1.

Modeling Assumptions We assume the observations \mathbf{Y}^{obs} are generated by a latent SCM ψ , representing the GRN of the given cell population. We consider single-node hard interventions $t \in \mathcal{T}$, where each treatment corresponds to a gene knockout modeled as $\text{do}(t)$ on the underlying causal structure. We assume \mathbf{Y}^{int} to stem from the intervened-upon SCM $\psi^{\text{do}(t)}$ and that all variables of the latent SCM are observed.

Given observational samples \mathbf{Y}^{obs} and a set of interventional experiments $\mathcal{C} = \{(t_k, \mathbf{Y}_k^{\text{int}})\}_{k=1}^K$ for ψ , we aim to directly predict the post-perturbation distribution of an unseen query treatment $t_q \in \mathcal{T} \setminus \mathcal{T}_C$. Based on our assumptions, the posterior predictive distribution takes the form

$$p(\mathbf{y}_q^{\text{int}} \mid \text{do}(t_q), \mathbf{Y}^{\text{obs}}, \mathcal{C}) = \int p(\mathbf{y}_q^{\text{int}} \mid \text{do}(t_q), \mathbf{Y}^{\text{obs}}, \psi) p(\psi \mid \mathbf{Y}^{\text{obs}}, \mathcal{C}) d\psi \quad (2)$$

MapPFN approximates this distribution by amortizing inference over diverse causal structures ψ sampled during synthetic pre-training. We refer to Robertson et al. (2025) for a theoretical discussion of the sources of uncertainty in this formulation.

Existing methods require a data split across multiple biological contexts and condition only on covariates or the observational distribution. In contrast, MapPFN conditions on interventional data of the context at hand through in-context learning. Additionally, existing models must be retrained on each new gene set, whereas MapPFN flexibly adapts to arbitrary gene sets through pre-training on *in silico* knockouts.

Pre-training Process During each pre-training step, we first sample an SCM $\psi \sim p(\psi)$ from the prior. By propagating noise $\mathbf{N} = [\epsilon_1, \dots, \epsilon_n]^\top$, $\epsilon_i \sim \mathcal{N}(0, \mathbf{I})$ through the SCM, we obtain the observational distribution \mathbf{Y}^{obs} . For the synthetic biological prior, we analogously simulate gene expression dynamics. Subsequently, we build the context $\mathcal{C} = \{(t_k, \mathbf{Y}_k^{\text{int}})\}_{k=1}^K$ by sampling SCMs $\psi^{\text{do}(t_k)}$ for a subset of treatments $t_k \in \mathcal{T}_C \subset \mathcal{T}$. For each intervention in this set, we generate post-perturbation distributions $\mathbf{Y}_k^{\text{int}}$ by drawing new noise \mathbf{N}_k . Finally, our prediction target is the post-perturbation distribution $\mathbf{Y}_q^{\text{int}}$ arising from an unseen query treatment $t_q \in \mathcal{T} \setminus \mathcal{T}_C$. Figure 1 provides an overview of MapPFN pre-training and inference. The full pre-training process is outlined in Algorithm 1.

Algorithm 1 MapPFN Pre-training

Input: prior $p(\psi)$, treatments \mathcal{T} , context size K
for $i = 1, 2, \dots, N$ **do**
 Draw SCM $\psi \sim p(\psi)$
 Draw observational samples $\mathbf{Y}^{\text{obs}} \sim p(\mathbf{y}^{\text{obs}} \mid \psi)$
 Draw context treatments $\mathcal{T}_C \subset \mathcal{T}$ with $|\mathcal{T}_C| = K$
 for $k = 1, \dots, K$ **do**
 Draw $\mathbf{Y}_k^{\text{int}} \sim p(\mathbf{y}^{\text{int}} \mid \text{do}(t_k), \psi)$
 end for
 Set context $\mathcal{C} \leftarrow \{(t_k, \mathbf{Y}_k^{\text{int}})\}_{k=1}^K$
 Draw query treatment $t_q \sim \mathcal{T} \setminus \mathcal{T}_C$
 Draw target $\mathbf{Y}_q^{\text{int}} \sim p(\mathbf{y}^{\text{int}} \mid \text{do}(t_q), \psi)$
 Draw time $\tau \sim \text{LogitNormal}(0, 1)$, $\mathbf{Y}_0 \sim \mathcal{N}(0, \mathbf{I})$
 Compute $\mathcal{L}_{\text{CFM}}(\theta; \mathbf{Y}_0, \tau, \mathbf{Y}_q^{\text{int}}, t_q, \mathbf{Y}^{\text{obs}}, \mathcal{C})$
 Update $\theta \leftarrow \theta - \alpha \nabla \mathcal{L}_{\text{CFM}}(\theta)$
end for

Note: $\mathbf{Y} \sim p(\mathbf{y} \mid \cdot, \psi)$ implies first sampling noise $\mathbf{N} \in \mathbb{R}^{n \times d}$ and stacking n i.i.d. samples.

Identifiability Perturbation prediction depends on identifiability, i.e. the extent to which the causal graph \mathcal{G}_ψ can be inferred from data, even if it is not explicitly recovered. Interventional data can fully identify the causal graph given sufficient interventions (Eberhardt et al., 2006). Conditioning on an interventional context \mathcal{C} reduces the Markov equivalence class $[\mathcal{G}_\psi]$, as each intervention constrains the set of causal structures consistent with the data (Hauser & Bühlmann, 2012). This provides MapPFN with a theoretical advantage over existing causal PFNs and perturbation models that learn from observational data alone, assuming the true causal graph lies within the support of the prior distribution $p(\psi)$.

4.1. Model

We adopt the Multimodal Diffusion Transformer (MMDiT; Esser et al., 2024) architecture with minor modifications. We treat cells as tokens, and input noise, cell states, and one-hot encoded treatments are processed as three modality streams with separate parameters. Cross-modal interactions are enabled via joint attention.

Because the inputs are unordered sets of cells, we remove sinusoidal positional encodings and rely on the permutation invariance of attention. Instead, we introduce learnable embeddings to differentiate modalities, query versus context, and observational versus interventional data. We train MapPFN using a conditional flow matching objective (Lipman et al., 2023), which learns a velocity field that transports noise to the predicted post-perturbation distribution.

$$\mathcal{L}_{\text{CFM}}(\theta) = \mathbb{E}_{\tau, \mathbf{Y}_0, \mathbf{Y}_q^{\text{int}}} \left\| v_\tau^\theta(\mathbf{Y}_\tau \mid t_q, \mathbf{Y}^{\text{obs}}, \mathcal{C}) - (\mathbf{Y}_q^{\text{int}} - \mathbf{Y}_0) \right\|_F^2 \quad (3)$$

where v_τ^θ is the learned velocity, $\mathbf{Y}_\tau = (1 - \tau)\mathbf{Y}_0 + \tau\mathbf{Y}_q^{\text{int}}$ is the interpolated sample at time τ , and θ denotes the model parameters. Please refer to Appendix A and Algorithm 1 for details on the model architecture and pre-training process.

5. Experimental Setup

We evaluate MapPFN in a controlled environment of known linear SCMs and on real-world single-cell perturbation datasets. We compare against baselines trained on the downstream datasets in three configurations: MapPFN trained from random initialization on real perturbation data, pre-trained on synthetic data, and fine-tuned on real data after synthetic pre-training.

5.1. Datasets

Linear Structural Causal Models We generate synthetic data from linear structural causal models (SCM) with additive Gaussian noise (Pearl, 2009). We sample directed acyclic graphs (DAGs) from an Erdős–Rényi distribution (Erdős & Rényi, 1960) with $d = 20$ nodes and an edge probability of $p = 0.5$. Additional details on the linear SCM data are provided in Appendix B.1.

Synthetic Biological Prior We first generate directed graphs from a scale-free distribution using the preferential attachment algorithm (Aguirre et al., 2025), allowing to generate networks with similar properties to real GRNs in terms of modularity, sparsity and degree distributions (see Appendix B.2).

Given a sampled regulatory network, we simulate single-cell gene expressions using SERGIO (Dibaecinia & Sinha, 2020), which models cell expressions as the steady state of a system of stochastic differential equations (SDEs). Regulatory interactions are parameterized by Hill functions (Gesztelyi et al., 2012), capturing nonlinear and saturation effects. Genetic perturbations are performed in-silico by removing the perturbed gene from the regulatory network and re-simulating the system. To obtain gene expression counts, we apply the technical noise model of SERGIO for 10x Chromium single-cell RNA sequencing. Additional details on the synthetic biological prior and its hyperparameters are provided in Appendix B.2.

Single-cell Perturbation Datasets Beyond the linear SCM setting, we evaluate on two biologically distinct single-cell perturbation datasets. The first (Frangieh et al., 2021) consists of approximately 218,000 cells from a CRISPR knockout screen of 248 genes in melanoma cells across three biological contexts. The second (Papalexli et al., 2021) consists of approximately 20,000 cells from a CRISPR perturbation screen of 26 genes in a leukemia cell line in a single biological context. Following Schneider et al. (2025),

Table 1. Overview of perturbation models by conditioning capability. Columns indicate whether a method conditions on covariates, observational populations, or interventional populations. MapPFN uniquely conditions on interventional data, leveraging perturbation responses measured in the target context via in-context learning.

Methods	Covariates	Observational	Interventional
CPA, CondOT, CellFlow	✓	✗	✗
MFM, STATE	✓	✓	✗
MapPFN (ours)	✓	✓	✓

we restrict analysis to 50 genes for both datasets. Additional details on the data are provided in Appendix B.3.

Data Split Our evaluation setting follows the Virtual Cell Challenge (Roohani et al., 2025), where adaptation to a new biological context is based on a limited number of interventional experiments. For linear SCM experiments, we train all methods including MapPFN on the same synthetic data. For the single-cell experiments, MapPFN is pre-trained on synthetic data and optionally fine-tuned on real perturbation data, while baselines are trained from scratch on real single-cell data, as they do not admit a similar pre-training phase. Additional details on the data split are provided in Appendix B.4.

5.2. Baselines

We compare our method against CPA (Lotfollahi et al., 2023), Conditional Optimal Transport (CondOT; Bunne et al., 2022), Meta Flow Matching (MFM; Atanackovic et al., 2025), CellFlow (Klein et al., 2025) and STATE (Aduri et al., 2025). While these baselines condition on covariates or observational populations at most, MapPFN is the only method that additionally conditions on interventional populations (Table 1). As lower and upper bounds, we report two reference baselines following Bunne et al. (2023): an identity baseline that predicts the observational distribution $\hat{\mathbf{y}}^{\text{int}} \sim p(\mathbf{y}^{\text{obs}})$, and an oracle baseline that uses the observed post-perturbation distribution $\hat{\mathbf{y}}^{\text{int}} \sim p(\mathbf{y}^{\text{int}})$. Additional details on the baselines are provided in subsection C.1.

5.3. Metrics

We evaluate perturbation prediction by comparing the predicted post-perturbation distribution $\hat{\mathbf{Y}}^{\text{int}}$ to the ground-truth distribution \mathbf{Y}^{int} in terms of distributional similarity, moment-level accuracy, perturbation distinguishability and differentially expressed gene (DEG) recovery. Distributional similarity is quantified using the entropy-regularized Wasserstein distance (W_2) (Cuturi, 2013) and the maximum mean discrepancy (MMD; Gretton et al., 2012). Moment-level accuracy is measured by the root mean squared error (RMSE) between the predicted and ground-truth distribution

Table 2. **Evaluation within a prior of linear SCMs.** Evaluation on synthetic data from known linear SCMs. Mean \pm std over three random seeds. Bold indicates results within one standard deviation of the best. In this controlled setting, MapPFN achieves best performance across all metrics.

Method	$W_2 \downarrow$	MMD ($\times 10^{-3}$) \downarrow	RMSE \downarrow	PDS \downarrow	MR
CondOT	13.85 \pm 0.12	5.14 \pm 0.01	0.15 \pm 0.00	0.11 \pm 0.02	0.09 \pm 0.01
MFM	13.73 \pm 0.16	4.81 \pm 0.19	0.15 \pm 0.01	0.09 \pm 0.03	0.12 \pm 0.00
MapPFN (ours)	13.69 \pm 0.05	4.28 \pm 0.06	0.14 \pm 0.00	0.01 \pm 0.01	0.99 \pm 0.02
Identity	17.61 \pm 0.14	12.98 \pm 0.35	0.28 \pm 0.01	0.49 \pm 0.01	0.00 \pm 0.00
Observed	9.82 \pm 0.08	3.66 \pm 0.06	0.07 \pm 0.00	0.00 \pm 0.00	1.00 \pm 0.00

means. To assess whether predictions are distinguishable across perturbations, we report the ranking-based perturbation discrimination score (PDS; Wu et al., 2025b). DEG recovery is evaluated using the area under the precision-recall curve (AUPRC) (Zhu et al., 2025), comparing DEGs from the predicted post-perturbation distribution with those observed in the ground-truth data. Additional details on the metrics are provided in subsection C.2.

Magnitude Ratio Causal effects can occur on different scales across biological contexts, making absolute distributional distances difficult to interpret. In particular, a small distance does not imply a weak causal effect, nor does a large distance imply a strong one. To normalize for effect scale, we introduce the *magnitude ratio* (MR), which measures how much of the true intervention effect is recovered by the prediction. Let d denote a distributional distance (e.g. Wasserstein distance). The magnitude ratio is defined as

$$\text{MR}(\mathbf{Y}^{\text{obs}}, \mathbf{Y}^{\text{int}}, \hat{\mathbf{Y}}^{\text{int}}) = \frac{d(\mathbf{Y}^{\text{obs}}, \hat{\mathbf{Y}}^{\text{int}})}{d(\mathbf{Y}^{\text{obs}}, \mathbf{Y}^{\text{int}})} \quad (4)$$

A perfect prediction corresponds to a magnitude ratio of 1.0 and an identity collapse ($\hat{\mathbf{Y}}^{\text{int}} = \mathbf{Y}^{\text{obs}}$) results in a magnitude ratio of 0.0. The magnitude ratio is invariant to the absolute effect scale and quantifies effect size recovery but not directionality. We report it using the Wasserstein distance.

6. Results

We report benchmarking results for linear SCMs in Table 2 and for single-cell datasets in Table 3. We ablate the interventional context and counterfactual paired prior in Table 4 and Figure 2, and demonstrate scaling to larger gene sets via test-time augmentation in Figure 3.

MapPFN achieves the best performance across all metrics on linear SCMs Table 2 compares MapPFN against CondOT and MFM within a prior of linear SCMs. MapPFN achieves the best performance across all metrics, only tied with MFM on Wasserstein distance. The magnitude ratio reveals identity collapse as a common failure mode in baselines. CondOT and MFM yield magnitude ratios around 0.1,

suggesting little deviation from the observational distribution, while MapPFN is the only method with a magnitude ratio close to one. We attribute this to both baselines either initializing the generative flow to the observational distribution or initializing the model weights as an identity map. These results show that MapPFN learns perturbation prediction in a controlled setting where the data-generating process is known, motivating evaluation on real single-cell data where the underlying causal structure is unknown.

Synthetic pre-training enables zero-shot recovery of differentially expressed genes Table 3 compares a single MapPFN pre-trained on the synthetic biological prior against baselines trained from scratch on two biologically distinct single-cell datasets. Zero-shot performance varies across datasets, with MapPFN achieving on-par AUPRC and the best MR on melanoma but worse distributional metrics on the leukemia dataset, which is less aligned with the synthetic prior in expression distribution (see Figure 6 in Appendix D). On both datasets, pre-trained MapPFN recovers differentially expressed genes zero-shot and on par with the best baselines trained on real perturbation data, as measured by AUPRC (Table 3). Identifying which genes are differentially expressed is critical for understanding treatment mechanisms and planning interventions.

Fine-tuned MapPFN consistently outperforms baselines across biological contexts Fine-tuned MapPFN achieves best PDS, MR and AUPRC on both datasets, and best performance on all metrics except W_2 on the leukemia dataset (Table 3). To isolate the contribution of synthetic pre-training, we compare fine-tuned MapPFN against a randomly initialized variant trained on the same real data. Random initialization performs worse on all metrics except W_2 across both datasets. These results suggest that meta-learning perturbation prediction on diverse synthetic causal mechanisms generalizes to real perturbation data across distinct biological contexts.

Interventional context improves performance over observational data alone We evaluate whether MapPFN benefits from improved identifiability by conditioning on interventional data. Specifically, we ablate the effect of

Table 3. Comparison of MapPFN against baselines trained on two single-cell perturbation datasets. Benchmark on a melanoma (Frangieh et al., 2021) and a leukemia (Papalexli et al., 2021) cell line. Ablations include MapPFN (1) trained from random initialization, (2) pre-trained on synthetic data and (3) fine-tuned on real data. Pre-trained MapPFN recovers differentially expressed genes on par with baselines trained on real data. Fine-tuned MapPFN consistently outperforms baselines across both datasets. Mean \pm std over ten resampling seeds. Bold indicates results within one standard deviation of the best.

Dataset	Method	$W_2 \downarrow$	MMD ($\times 10^{-3}$) \downarrow	RMSE \downarrow	PDS \downarrow	MR	AUPRC \uparrow
Melanoma	CPA	15.57 \pm 0.10	140.09 \pm 0.35	0.13 \pm 0.00	0.49 \pm 0.01	0.68 \pm 0.01	0.04 \pm 0.00
	CondOT	22.09 \pm 0.39	7.11 \pm 0.12	0.10 \pm 0.00	0.06 \pm 0.01	0.05 \pm 0.00	0.34 \pm 0.05
	MFM	20.99 \pm 0.14	7.28 \pm 0.13	0.10 \pm 0.00	0.09 \pm 0.02	0.13 \pm 0.00	0.28 \pm 0.04
	CellFlow	22.27 \pm 0.59	7.16 \pm 0.17	0.10 \pm 0.00	0.41 \pm 0.01	0.01 \pm 0.00	0.10 \pm 0.02
	STATE	20.52 \pm 0.07	7.82 \pm 0.09	0.08 \pm 0.00	0.07 \pm 0.02	0.94 \pm 0.00	0.33 \pm 0.04
	MapPFN (random init)	21.23 \pm 0.11	51.78 \pm 0.80	0.24 \pm 0.00	0.18 \pm 0.02	1.02 \pm 0.01	0.12 \pm 0.02
	MapPFN (pre-trained)	22.75 \pm 0.16	10.07 \pm 0.19	0.13 \pm 0.00	0.17 \pm 0.01	1.00 \pm 0.01	0.34 \pm 0.02
	MapPFN (fine-tuned)	21.38 \pm 0.12	7.84 \pm 0.14	0.10 \pm 0.00	0.03 \pm 0.01	0.99 \pm 0.00	0.38 \pm 0.03
	Identity	22.91 \pm 0.18	7.90 \pm 0.17	0.11 \pm 0.00	0.51 \pm 0.02	0.00 \pm 0.00	0.04 \pm 0.01
	Observed	8.54 \pm 0.10	2.59 \pm 0.07	0.04 \pm 0.00	0.00 \pm 0.00	1.00 \pm 0.00	0.64 \pm 0.06
Leukemia	CPA	12.41 \pm 0.11	78.74 \pm 1.27	0.17 \pm 0.00	0.50 \pm 0.02	0.61 \pm 0.01	0.15 \pm 0.01
	CondOT	17.92 \pm 0.37	26.51 \pm 0.68	0.27 \pm 0.01	0.54 \pm 0.04	0.19 \pm 0.00	0.14 \pm 0.01
	MFM	41.71 \pm 0.26	105.64 \pm 0.73	0.71 \pm 0.00	0.51 \pm 0.02	1.67 \pm 0.01	0.16 \pm 0.01
	CellFlow	16.87 \pm 0.37	14.55 \pm 0.46	0.17 \pm 0.00	0.50 \pm 0.01	0.02 \pm 0.00	0.16 \pm 0.01
	STATE	15.27 \pm 0.15	15.28 \pm 0.44	0.17 \pm 0.00	0.47 \pm 0.03	0.83 \pm 0.00	0.17 \pm 0.01
	MapPFN (random init)	14.95 \pm 0.28	24.47 \pm 0.90	0.19 \pm 0.01	0.54 \pm 0.02	0.82 \pm 0.01	0.16 \pm 0.01
	MapPFN (pre-trained)	44.42 \pm 0.23	191.88 \pm 1.46	0.78 \pm 0.00	0.49 \pm 0.01	2.56 \pm 0.02	0.16 \pm 0.01
	MapPFN (fine-tuned)	16.32 \pm 0.11	12.24 \pm 0.58	0.15 \pm 0.00	0.42 \pm 0.03	0.91 \pm 0.01	0.18 \pm 0.01
	Identity	16.72 \pm 0.18	13.17 \pm 0.44	0.14 \pm 0.01	0.49 \pm 0.02	0.00 \pm 0.00	0.18 \pm 0.01
	Observed	10.29 \pm 0.12	2.59 \pm 0.04	0.04 \pm 0.00	0.03 \pm 0.02	0.99 \pm 0.01	0.91 \pm 0.04

providing a set of interventional distributions \mathcal{C} versus the observational-only setting, where $\mathcal{C} = \emptyset$. As shown in Table 4, conditioning on interventional distributions improves performance across all metrics over using only observational data. Since the model architecture remains unchanged, this gain can be attributed to the interventional context rather than architectural differences. This suggests that interventional context enables MapPFN to learn perturbation-specific mappings not accessible from observational data alone. Performance further improves monotonically with the number of interventional experiments provided in context (see Figure 5a in Appendix D).

Counterfactual paired prior improves downstream performance

Since individual cells are destroyed during measurement, perturbation data is unpaired across treatments. To isolate the task of causal inference from the additional difficulty introduced by unpaired data, we follow Robertson et al. (2025) and pre-train MapPFN on counterfactual interventional data, achieved by keeping the random seed of SERGIO constant across treatments. This ensures that the differences between interventional distributions are not driven by a difference in initial condition to the stochastic differential equation, but only by the differences in underlying mechanism and perturbation effects. Figure 2 shows the Pearson correlation between the feature-wise variances of the predicted and ground-truth post-perturbation distribu-

tion on the validation set, evaluated separately for the paired and unpaired prior. The paired prior converges to a variance correlation of approximately 0.8 within 50k steps, while the unpaired prior saturates around 0.6 even after 400k steps. The paired prior results in a substantial improvement across all metrics on real single-cell data (Table 4). We suspect that counterfactual interventional distributions provide stronger signal by isolating causal effects from the added variability of unpaired samples.

MapPFN adapts to larger gene sets and number of cells at inference time

Pre-trained on *in silico* knockouts, MapPFN uniquely adapts to arbitrary gene sets at inference time without retraining. To scale beyond the 50 genes seen during training, we apply test-time augmentation (TTA). We sample random overlapping subsets of 50 genes from 100, predict cell-level post-perturbation distributions for each subset, pool predicted cells per gene across subsets, and identify differentially expressed genes via per-gene statistical testing. As shown in Figure 3, TTA improves AUPRC and reduces its variance across resampling seeds, indicating that MapPFN generalizes to larger gene sets with more stable predictions. Performance also improves beyond the training configuration with more cells per perturbation in context, showing that MapPFN adapts predictions to the data via in-context learning (see Figure 5b in Appendix D).

Table 4. Ablation of the counterfactual paired prior and interventional context on the melanoma dataset. Removing the paired prior replaces counterfactual data with unpaired interventional distributions. Removing the interventional context implies conditioning only on observational data ($C = \emptyset$). Both ablations degrade performance across all metrics. Mean \pm std over ten resampling seeds. Bold indicates results within one standard deviation of the best.

	$W_2 \downarrow$	MMD ($\times 10^{-3}$) \downarrow	RMSE \downarrow	PDS \downarrow	MR	AUPRC \uparrow
MapPFN (pre-trained)	22.75 \pm 0.16	10.07 \pm 0.19	0.13 \pm 0.00	0.17 \pm 0.01	1.00 \pm 0.01	0.34 \pm 0.02
– paired prior	24.44 \pm 0.31	21.84 \pm 1.28	0.23 \pm 0.01	0.20 \pm 0.02	1.14 \pm 0.01	0.21 \pm 0.03
– interventional context	23.78 \pm 0.16	15.88 \pm 0.19	0.20 \pm 0.00	0.20 \pm 0.01	1.10 \pm 0.01	0.13 \pm 0.02

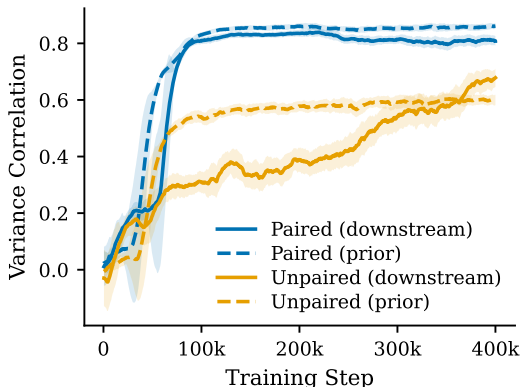


Figure 2. Counterfactual paired prior improves downstream performance. The paired prior converges faster and to higher performance than the unpaired prior, both within the prior (dashed) and on real single-cell data (solid). Variance correlation measures the Pearson correlation between feature variances of predicted and ground-truth samples. Shaded regions indicate rolling standard deviation; curves show EMA ($\alpha = 0.95$).

7. Discussion

We introduced MapPFN, the first prior-data fitted network for perturbation prediction, framing the problem as in-context learning over interventional distributions. Pre-trained on synthetic perturbation data, MapPFN is not limited by the number of experimentally measured biological contexts.

Pre-trained exclusively on synthetic perturbations, MapPFN recovers differentially expressed genes in real single-cell data on par with baselines trained on real perturbations. Fine-tuned on real data, MapPFN consistently outperforms baselines across downstream datasets. These results suggest that pre-training on diverse synthetic causal mechanisms enables meta-learning perturbation prediction. MapPFN uniquely adapts to arbitrary gene sets at inference time via test-time augmentation. We find that conditioning on interventional experiments improves prediction of unseen perturbations compared to methods that condition only on covariates or the observational distribution. We attribute this to improved identifiability, as the interventional context helps reduce the Markov equivalence class of the underlying causal mechanisms.

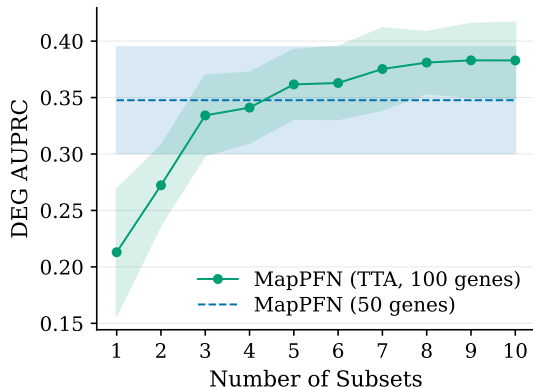


Figure 3. MapPFN scales to larger gene sets via test-time augmentation. MapPFN (TTA) aggregates predictions over ten random overlapping subsets of 50 genes drawn from 100 genes, improving recovery of differentially expressed genes as measured by AUPRC with more stable predictions. Shaded areas indicate standard deviation over ten resampling seeds.

Limitations While pre-training on synthetic data allows MapPFN to scale beyond the few biological contexts covered by current perturbation datasets, its ability to generalize depends on the synthetic biological prior. Future work should investigate to which extent counterfactual priors may be preferable and how to systematically evaluate them. While MapPFN can adapt to larger gene sets through test-time augmentation, scaling to larger input dimensions offers a promising direction (Kolberg et al., 2025). While MapPFN adapts to new datasets in minutes, pre-training on synthetic data comes at a one-time cost of 36 GPU hours. Finally, extending MapPFN to support combinatorial, drug-based or chemical perturbations remains an open challenge (Schneider et al., 2025; Dong et al., 2026; Wu et al., 2025a).

Outlook Given the success of PFNs in tabular prediction and causal inference, we anticipate that scaling MapPFN in terms of model capacity and extending the synthetic prior to more diverse regulatory mechanisms and broader perturbation types will yield further improvements. Our findings suggest that meta-learning perturbation prediction on synthetic biological priors with test-time interventional context offers a scalable path toward context-adaptive virtual cell foundation models.

Acknowledgements

The authors would like to thank Michael Plainer, Jonas Loos and Alexander Möllers for the fruitful discussions and helpful input.

Impact Statement

This work advances machine learning methods for predicting perturbation effects. While our approach shows promise in complementing experimental validation by helping to prioritize hypotheses in research settings, substantial further development and validation would be required before any clinical applications. We do not believe there are societal or scientific consequences of this work that must be specifically highlighted here beyond its contribution to the field of machine learning.

References

- Adduri, A. K., Gautam, D., Bevilacqua, B., Imran, A., Shah, R., Naghipourfar, M., Teyssier, N., Ilango, R., Nagaraj, S., Dong, M., Ricci-Tam, C., Carpenter, C., Subramanyam, V., Winters, A., Tirukkovular, S., Sullivan, J., Plosky, B. S., Eraslan, B., Youngblut, N. D., Leskovec, J., Gilbert, L. A., Konermann, S., Hsu, P. D., Dobin, A., Burke, D. P., Goodarzi, H., and Roohani, Y. H. Predicting cellular responses to perturbation across diverse contexts with State. *bioRxiv:10.1101/2025.06.26.661135*, 2025.
- Aguirre, M., Spence, J. P., Sella, G., and Pritchard, J. K. Gene regulatory network structure informs the distribution of perturbation effects. *PLOS Computational Biology*, 21(9):1–31, 2025.
- Amos, B., Xu, L., and Kolter, J. Z. Input convex neural networks. In *Proceedings of the 34th International Conference on Machine Learning*, volume 70 of *Proceedings of Machine Learning Research*, pp. 146–155, 2017.
- Amos, B., Luise, G., Cohen, S., and Redko, I. Meta optimal transport. In *Proceedings of the 40th International Conference on Machine Learning*, volume 202 of *Proceedings of Machine Learning Research*, pp. 791–813, 2023.
- Atanackovic, L., Zhang, X. N., Amos, B., Blanchette, M., Lee, L. J., Bengio, Y., Tong, A., and Neklyudov, K. Meta Flow Matching: Integrating Vector Fields on the Wasserstein Manifold. In *International Conference on Learning Representations*, volume 2025, pp. 94586–94610, 2025.
- Balazadeh, V., Kamkari, H., Thomas, V., Li, B., Ma, J., Cresswell, J. C., and Krishnan, R. G. CausalPFN: Amortized causal effect estimation via in-context learning. In *Advances in Neural Information Processing Systems*, volume 38, 2025.
- Benjamini, Y. and Hochberg, Y. On the adaptive control of the false discovery rate in multiple testing with independent statistics. *Journal of Educational and Behavioral Statistics*, 25(1):60–83, 2000.
- Bradbury, J., Frostig, R., Hawkins, P., Johnson, M. J., Leary, C., Maclaurin, D., Necula, G., Paszke, A., VanderPlas, J., Wanderman-Milne, S., and Zhang, Q. JAX: composable transformations of Python+NumPy programs, 2018.
- Brown, T., Mann, B., Ryder, N., Subbiah, M., Kaplan, J. D., Dhariwal, P., Neelakantan, A., Shyam, P., Sastry, G., Askell, A., Agarwal, S., Herbert-Voss, A., Krueger, G., Henighan, T., Child, R., Ramesh, A., Ziegler, D., Wu, J., Winter, C., Hesse, C., Chen, M., Sigler, E., Litwin, M., Gray, S., Chess, B., Clark, J., Berner, C., McCandlish, S., Radford, A., Sutskever, I., and Amodei, D. Language Models are Few-Shot Learners. In *Advances in Neural Information Processing Systems*, volume 33, pp. 1877–1901, 2020.
- Bunne, C., Krause, A., and Cuturi, M. Supervised Training of Conditional Monge Maps. In *Advances in Neural Information Processing Systems*, volume 35, pp. 6859–6872, 2022.
- Bunne, C., Stark, S. G., Gut, G., del Castillo, J. S., Levesque, M., Lehmann, K.-V., Pelkmans, L., Krause, A., and Rätsch, G. Learning single-cell perturbation responses using neural optimal transport. *Nature Methods*, 20(11):1759–1768, 2023.
- Bunne, C., Roohani, Y., Rosen, Y., Gupta, A., Zhang, X., Roed, M., Alexandrov, T., AlQuraishi, M., Brennan, P., Burkhardt, D. B., Califano, A., Cool, J., Dernburg, A. F., Ewing, K., Fox, E. B., Hauray, M., Herr, A. E., Horvitz, E., Hsu, P. D., Jain, V., Johnson, G. R., Kalil, T., Kelley, D. R., Kelley, S. O., Kreshuk, A., Mitchison, T., Otte, S., Shendure, J., Sofroniew, N. J., Theis, F., Theodoris, C. V., Upadhyayula, S., Valer, M., Wang, B., Xing, E., Yeung-Levy, S., Zitnik, M., Karaletsos, T., Regev, A., Lundberg, E., Leskovec, J., and Quake, S. R. How to build the virtual cell with artificial intelligence: Priorities and opportunities. *Cell*, 187(25):7045–7063, 2024.
- Butkus, E. and Kriegeskorte, N. Causal discovery and inference through next-token prediction. In *The Thirty-ninth Annual Conference on Neural Information Processing Systems*, 2025.
- Chatzaroulas, E. sergio_rs: The SERGIO v2 simulator rewritten in Rust, 2024. URL https://github.com/rainx0r/sergio_rs.
- Cui, H., Wang, C., Maan, H., Pang, K., Luo, F., Duan, N., and Wang, B. scGPT: toward building a foundation model for single-cell multi-omics using generative AI. *Nature Methods*, 21(8):1470–1480, 2024.

- Cuturi, M. Sinkhorn Distances: Lightspeed Computation of Optimal Transport. In *Advances in Neural Information Processing Systems*, volume 26, 2013.
- Cuturi, M., Meng-Papaxanthos, L., Tian, Y., Bunne, C., Davis, G., and Teboul, O. Optimal Transport Tools (OTT): A JAX Toolbox for all things Wasserstein. *arXiv:2201.12324*, 2022.
- Dhir, A., Ashman, M., Requeima, J., and van der Wilk, M. A meta-learning approach to bayesian causal discovery. In *The Thirteenth International Conference on Learning Representations*, 2025.
- Dibaenia, P. and Sinha, S. SERGIO: A Single-Cell Expression Simulator Guided by Gene Regulatory Networks. *Cell Systems*, 11(3):252–271, 2020.
- Dixit, A., Parnas, O., Li, B., Chen, J., Fulco, C. P., Jerby-Arnon, L., Marjanovic, N. D., Dionne, D., Burks, T., Raychdhury, R., Adamson, B., Norman, T. M., Lander, E. S., Weissman, J. S., Friedman, N., and Regev, A. Perturb-seq: Dissecting molecular circuits with scalable single cell RNA profiling of pooled genetic screens. *Cell*, 167(7):1853–1866, 2016.
- Dong, M., Wang, B., Wei, J., de O. Fonseca, A. H., Perry, C. J., Frey, A., Ouerghi, F., Foxman, E. F., Ishizuka, J. J., Dhodapkar, R. M., and van Dijk, D. Causal identification of single-cell experimental perturbation effects with CINEMA-OT. *Nature Methods*, 20(11):1769–1779, 2023.
- Dong, M., Adduri, A., Gautam, D., Carpenter, C., Shah, R., Ricci-Tam, C., Kluger, Y., Burke, D. P., and Roohani, Y. H. Stack: In-Context Learning of Single-Cell Biology. *bioRxiv:10.64898/2026.01.09.698608*, 2026.
- Dormand, J. R. and Prince, P. J. A family of embedded Runge-Kutta formulae. *Journal of Computational and Applied Mathematics*, 6(1):19–26, 1980.
- Dremov, A., Hägele, A., Kosson, A., and Jaggi, M. Training dynamics of the cooldown stage in warmup-stable-decay learning rate scheduler. *Transactions on Machine Learning Research*, 2025.
- Eberhardt, F., Glymour, C., and Scheines, R. N-1 Experiments Suffice to Determine the Causal Relations Among N Variables. In *Innovations in Machine Learning: Theory and Applications*, pp. 97–112. Springer Berlin Heidelberg, 2006.
- Erdős, P. and Rényi, A. On the evolution of random graphs. *Publications of the Mathematical Institute of the Hungarian Academy of Sciences*, 5(1):17–60, 1960.
- Esser, P., Kulal, S., Blattmann, A., Entezari, R., Müller, J., Saini, H., Levi, Y., Lorenz, D., Sauer, A., Boesel, F., Podell, D., Dockhorn, T., English, Z., and Rombach, R. Scaling rectified flow transformers for high-resolution image synthesis. In *Proceedings of the 41st International Conference on Machine Learning*, volume 235 of *Proceedings of Machine Learning Research*, pp. 12606–12633, 2024.
- Feydy, J., Séjourné, T., Vialard, F.-X., Amari, S.-i., Trounev, A., and Peyré, G. Interpolating between optimal transport and mmd using sinkhorn divergences. In *Proceedings of the Twenty-Second International Conference on Artificial Intelligence and Statistics*, volume 89 of *Proceedings of Machine Learning Research*, pp. 2681–2690, 2019.
- Frangieh, C. J., Melms, J. C., Thakore, P. I., Geiger-Schuller, K. R., Ho, P., Luoma, A. M., Cleary, B., Jerby-Arnon, L., Malu, S., Cuoco, M. S., Zhao, M., Ager, C. R., Rogava, M., Hovey, L., Rotem, A., Bernatchez, C., Wucherpennig, K. W., Johnson, B. E., Rozenblatt-Rosen, O., Schadendorf, D., Regev, A., and Izar, B. Multimodal pooled Perturb-CITE-seq screens in patient models define mechanisms of cancer immune evasion. *Nature Genetics*, 53(3):332–341, 2021.
- Genevay, A., Peyre, G., and Cuturi, M. Learning generative models with sinkhorn divergences. In *Proceedings of the Twenty-First International Conference on Artificial Intelligence and Statistics*, volume 84 of *Proceedings of Machine Learning Research*, pp. 1608–1617, 09–11 Apr 2018.
- Gesztelyi, R., Zsuga, J., Kemeny-Beke, A., Varga, B., Juhasz, B., and Tosaki, A. The Hill equation and the origin of quantitative pharmacology. *Archive for History of Exact Sciences*, 66(4):427–438, 2012.
- Gillespie, D. T. The chemical Langevin equation. *The Journal of Chemical Physics*, 113(1):297–306, 2000.
- Gretton, A., Borgwardt, K. M., Rasch, M. J., Schölkopf, B., and Smola, A. A Kernel Two-Sample Test. *Journal of Machine Learning Research*, 13(25):723–773, 2012.
- Hao, M., Gong, J., Zeng, X., Liu, C., Guo, Y., Cheng, X., Wang, T., Ma, J., Zhang, X., and Song, L. Large-scale foundation model on single-cell transcriptomics. *Nature Methods*, 21(8):1481–1491, 2024.
- Hauser, A. and Bühlmann, P. Characterization and Greedy Learning of Interventional Markov Equivalence Classes of Directed Acyclic Graphs. *Journal of Machine Learning Research*, 13(79):2409–2464, 2012.
- Heumos, L., Ji, Y., May, L., Green, T. D., Peidli, S., Zhang, X., Wu, X., Ostner, J., Schumacher, A., Hrovatin, K.,

- Müller, M., Chong, F., Sturm, G., Tejada, A., Dann, E., Dong, M., Pinto, G., Bahrami, M., Gold, I., Rybakov, S., Namsaraeva, A., Moinfar, A. A., Zheng, Z., Roellin, E., Mekki, I., Sander, C., Lotfollahi, M., Schiller, H. B., and Theis, F. J. Pertpy: an end-to-end framework for perturbation analysis. *Nature Methods*, 2025.
- Ho, J. and Salimans, T. Classifier-free diffusion guidance. *arXiv:2207.12598*, 2021.
- Hollmann, N., Müller, S., Eggensperger, K., and Hutter, F. TabPFN: A transformer that solves small tabular classification problems in a second. In *The Eleventh International Conference on Learning Representations*, 2023.
- Hollmann, N., Müller, S., Purucker, L., Krishnakumar, A., Körfer, M., Hoo, S. B., Schirrmeyer, R. T., and Hutter, F. Accurate predictions on small data with a tabular foundation model. *Nature*, 637(8045):319–326, 2025.
- Jinek, M., Chylinski, K., Fonfara, I., Hauer, M., Doudna, J. A., and Charpentier, E. A Programmable Dual-RNA-Guided DNA Endonuclease in Adaptive Bacterial Immunity. *Science*, 337(6096):816–821, 2012.
- Ke, N. R., Chiappa, S., Wang, J. X., Bornschein, J., Goyal, A., Rey, M., Weber, T., Botvinick, M., Mozer, M. C., and Rezende, D. J. Learning to induce causal structure. In *International Conference on Learning Representations*, 2023.
- Kidger, P. On Neural Differential Equations. *arXiv:2202.02435*, 2022.
- Kidger, P. and Garcia, C. Equinox: neural networks in JAX via callable PyTrees and filtered transformations. *Differentiable Programming workshop at Neural Information Processing Systems 2021*, 2021.
- Klein, D., Uscidda, T., Theis, F., and Cuturi, M. GENOT: Entropic (Gromov) Wasserstein Flow Matching with Applications to Single-Cell Genomics. In *Advances in Neural Information Processing Systems*, volume 37, pp. 103897–103944, 2024.
- Klein, D., Fleck, J. S., Bobrovskiy, D., Zimmermann, L., Becker, S., Palma, A., Dony, L., Tejada-Lapueta, A., Huguët, G., Lin, H.-C., Azbukina, N., Sanchís-Calleja, F., Uscidda, T., Szalata, A., Gander, M., Regev, A., Treutlein, B., Camp, J. G., and Theis, F. J. CellFlow enables generative single-cell phenotype modeling with flow matching. *bioRxiv:10.1101/2025.04.11.648220*, 2025.
- Kolberg, C., Eggensperger, K., and Pfeifer, N. TabPFN-Wide: Continued Pre-Training for Extreme Feature Counts. *arXiv:2510.06162*, 2025.
- Lipman, Y., Chen, R. T. Q., Ben-Hamu, H., Nickel, M., and Le, M. Flow matching for generative modeling. In *The Eleventh International Conference on Learning Representations*, 2023.
- Lorch, L., Sussex, S., Rothfuss, J., Krause, A., and Schölkopf, B. Amortized Inference for Causal Structure Learning. In *Advances in Neural Information Processing Systems*, volume 35, pp. 13104–13118, 2022.
- Loshchilov, I. and Hutter, F. Decoupled weight decay regularization. In *International Conference on Learning Representations*, 2019.
- Lotfollahi, M., Klimovskaia Susmelj, A., De Donno, C., Hetzel, L., Ji, Y., Ibarra, I. L., Srivatsan, S. R., Naghipourfar, M., Daza, R. M., Martin, B., Shendure, J., McFaline-Figueroa, J. L., Boyeau, P., Wolf, F. A., Yakubova, N., Günemann, S., Trapnell, C., Lopez-Paz, D., and Theis, F. J. Predicting cellular responses to complex perturbations in high-throughput screens. *Molecular Systems Biology*, 19(6), 2023.
- Luecken, M. D. and Theis, F. J. Current best practices in single-cell RNA-seq analysis: a tutorial. *Molecular Systems Biology*, 15(6), 2019.
- Ma, Y., Frauen, D., Javurek, E., and Feuerriegel, S. Foundation Models for Causal Inference via Prior-Data Fitted Networks. *arXiv:2506.10914*, 2025.
- Müller, S., Hollmann, N., Arango, S. P., Grabocka, J., and Hutter, F. Transformers can do bayesian inference. In *International Conference on Learning Representations*, 2022.
- Müller, S., Feuer, M., Hollmann, N., and Hutter, F. PFNs4BO: In-context learning for Bayesian optimization. In *Proceedings of the 40th International Conference on Machine Learning*, volume 202 of *Proceedings of Machine Learning Research*, pp. 25444–25470, 2023.
- Papalexli, E., Mimitou, E. P., Butler, A. W., Foster, S., Bracken, B., Mauck, W. M., Wessels, H.-H., Hao, Y., Yeung, B. Z., Smibert, P., and Satija, R. Characterizing the molecular regulation of inhibitory immune checkpoints with multimodal single-cell screens. *Nature Genetics*, 53(3):322–331, 2021.
- Pearl, J. *Causality*. Cambridge University Press, 2009.
- Perez, E., Strub, F., de Vries, H., Dumoulin, V., and Courville, A. FiLM: Visual Reasoning with a General Conditioning Layer. *Proceedings of the AAAI Conference on Artificial Intelligence*, 32(1), 2018.
- Qu, J., Holzmüller, D., Varoquaux, G., and Le Morvan, M. TabICL: A tabular foundation model for in-context

- learning on large data. In *Proceedings of the 42nd International Conference on Machine Learning*, volume 267 of *Proceedings of Machine Learning Research*, pp. 50817–50847. PMLR, 2025.
- Reisach, A., Seiler, C., and Weichwald, S. Beware of the Simulated DAG! Causal Discovery Benchmarks May Be Easy to Game. In *Advances in Neural Information Processing Systems*, volume 34, pp. 27772–27784, 2021.
- Reuter, A., Rudner, T. G. J., Fortuin, V., and Rügamer, D. Can transformers learn full Bayesian inference in context? In *Proceedings of the 42nd International Conference on Machine Learning*, volume 267 of *Proceedings of Machine Learning Research*, pp. 51531–51582, 2025.
- Robertson, J., Reuter, A., Guo, S., Hollmann, N., Hutter, F., and Schölkopf, B. Do-PFN: In-Context Learning for Causal Effect Estimation. In *Advances in Neural Information Processing Systems*, volume 39, 2025.
- Roohani, Y., Huang, K., and Leskovec, J. Predicting transcriptional outcomes of novel multigene perturbations with GEARS. *Nature Biotechnology*, 42(6):927–935, 2024.
- Roohani, Y. H., Hua, T. J., Tung, P.-Y., Bounds, L. R., Yu, F. B., Dobin, A., Teyssier, N., Adduri, A., Woodrow, A., Plosky, B. S., Mehta, R., Hsu, B., Sullivan, J., Ricci-Tam, C., Li, N., Kazaks, J., Gilbert, L. A., Konermann, S., Hsu, P. D., Goodarzi, H., and Burke, D. P. Virtual Cell Challenge: Toward a Turing test for the virtual cell. *Cell*, 188(13):3370–3374, 2025.
- Sachs, K., Perez, O., Pe’er, D., Lauffenburger, D. A., and Nolan, G. P. Causal Protein-Signaling Networks Derived from Multiparameter Single-Cell Data. *Science*, 308(5721):523–529, 2005.
- Schneider, N., Lorch, L., Kilbertus, N., Schölkopf, B., and Krause, A. Generative intervention models for causal perturbation modeling. In *Proceedings of the 42nd International Conference on Machine Learning*, volume 267 of *Proceedings of Machine Learning Research*, pp. 53388–53412, 2025.
- Soklaski, R., Goodwin, J., Brown, O., Yee, M., and Matterer, J. Tools and Practices for Responsible AI Engineering. *arXiv:2201.05647*, 2022.
- Theodoris, C. V., Xiao, L., Chopra, A., Chaffin, M. D., Al Sayed, Z. R., Hill, M. C., Mantineo, H., Brydon, E. M., Zeng, Z., Liu, X. S., and Ellinor, P. T. Transfer learning enables predictions in network biology. *Nature*, 618(7965):616–624, 2023.
- Vapnik, V. *Estimation of Dependences Based on Empirical Data*. Springer, 2006.
- Virshup, I., Rybakov, S., Theis, F. J., Angerer, P., and Wolf, F. A. anndata: Access and store annotated data matrices. *Journal of Open Source Software*, 9(101):4371, 2024.
- Wilcoxon, F. Individual comparisons by ranking methods. *Biometrics Bulletin*, 1(6):80–83, 1945.
- Wolf, F. A., Angerer, P., and Theis, F. J. SCANPY: large-scale single-cell gene expression data analysis. *Genome Biology*, 19(1):15, 2018.
- Wu, M., Padia, U., Murphy, S. H., Barzilay, R., and Jaakkola, T. Identifying biological perturbation targets through causal differential networks. In *Proceedings of the 42nd International Conference on Machine Learning*, volume 267 of *Proceedings of Machine Learning Research*, pp. 67537–67561, 2025a.
- Wu, Y., Wershof, E., Schmon, S. M., Nassar, M., Osiński, B., Eksi, R., Yan, Z., Stark, R., Zhang, K., and Graepel, T. PerturBench: Benchmarking Machine Learning Models for Cellular Perturbation Analysis. In *Advances in Neural Information Processing Systems*, volume 39, 2025b.
- Zhang, J., Ubas, A. A., Borja, R. d., Svensson, V., Thomas, N., Thakar, N., Lai, I., Winters, A., Khan, U., Jones, M. G., Thompson, J. D., Tran, V., Pangallo, J., Papalexi, E., Sapre, A., Nguyen, H., Sander-son, O., Nigos, M., Kaplan, O., Schroeder, S., Hari-adi, B., Marrujo, S., Salvino, C. C. A., Olivares, G. G., Koehler, R., Geiss, G., Rosenberg, A., Roco, C., Merico, D., Alidoust, N., Goodarzi, H., and Yu, J. Tahoe-100M: A Giga-Scale Single-Cell Perturbation Atlas for Context-Dependent Gene Function and Cellular Model-ling. *bioRxiv:10.1101/2025.02.20.639398*, 2025.
- Zhu, H., Asiaee, A., Azinfar, L., Li, J., Liang, H., Irajizad, E., Do, K.-A., and Long, J. P. AUPRC: a metric for evaluating the performance of in-silico perturbation methods in identifying differentially expressed genes. *Briefings in Bioinformatics*, 26(5):bbaf426, 2025.

Appendix

A Model	13
A.1 Architecture	13
A.2 Pre-training	13
A.3 Fine-tuning	14
A.4 Inference	14
B Datasets	14
B.1 Linear Additive Noise Models	14
B.2 Synthetic Biological Prior	14
B.3 Single-cell Perturbation Datasets	15
B.4 Data Split	16
C Experimental Details	16
C.1 Baselines	16
C.2 Metrics	17
C.3 Hyperparameters	18
C.4 Implementation	19
D Additional Results	19
D.1 Test-time Scaling	19
D.2 Prior Coverage	19

A. Model

A.1. Architecture

We build on the Multi-modal Diffusion Transformer (MMDiT; Esser et al., 2024) architecture from the Stable Diffusion 3 family. Instead of text and image modalities, we keep the denoising process, the pre- and post-treatment data as well as the treatment in three modality streams. With this setup, each modality has separate weights and information flows between modalities via joint attention. As we are working with sets of cells, we use the permutation invariance of the attention mechanism by removing the sinusoid positional encoding. Instead, we add learnable embeddings (a) for each treatment in the context to tell apart different conditions, (b) to tell apart observational and interventional data, and (c) to tell apart the query condition from the context. Our model has 8 layers with an embedding dimension of 256 and a $2\times$ expansion to 512 in the feed-forward layers. We append 8 register tokens to the noise stream and use 4 multi-head attention heads of size 64 each. Time conditioning is implemented by Feature-wise Linear Modulation (FiLM; Perez et al., 2018). Overall, this configuration amounts to approximately 25M trainable parameters.

A.2. Pre-training

We pre-train our model using a flow matching (Lipman et al., 2023) objective with an affine Gaussian probability path. During training, we randomly drop the condition by replacing it with a learnable `null` embedding with probability $p = 0.2$. Following Esser et al. (2024), we sample $t \sim \text{LogitNormal}(0, 1)$. We use the AdamW optimizer (Loshchilov & Hutter, 2019) with a warmup-stable-decay learning rate schedule (Dremov et al., 2025) using 1% of the total number of steps for warmup to a peak learning rate of 10^{-4} and 20% for a square root decay. We maintain an exponential moving average

(EMA) of model weights with a decay of 0.999 and use these weights for inference (Esser et al., 2024). We pre-train for 50k steps on the linear SCM prior and 400k steps on the synthetic biological prior.

A.3. Fine-tuning

We fine-tune MapPFN for 3,000 iterations with a linear warmup to a reduced peak learning rate of 5×10^{-5} , taking approximately 10 minutes on a single GPU.

A.4. Inference

To generate samples, we integrate the learned flow by solving its ordinary differential equation (ODE) using the Dopri5 (Dormand & Prince, 1980) solver, as implemented in `diffraX` (Kidger, 2022). We use classifier-free guidance (Ho & Salimans, 2021) for conditional generation with a guidance weight $\omega = 2.0$ by default.

B. Datasets

B.1. Linear Additive Noise Models

Structural Causal Model We generate synthetic observational and interventional data using a linear additive noise model (ANM) with Gaussian noise of the form $\mathbf{z} = \mathbf{W}\mathbf{z} + \epsilon$, where $\mathbf{W} \in \mathbb{R}^{d \times d}$ is a weighted adjacency matrix encoding the causal graph and $\epsilon \sim \mathcal{N}(0, \mathbf{I})$ represents independent additive noise. The underlying directed acyclic graph (DAG) is sampled from an Erdős-Rényi (Erdős & Rényi, 1960) model $\mathcal{G}(d, p)$ with $d = 20$ nodes and an edge probability of $p = 0.5$, restricted to the upper triangular structure under a random node permutation to ensure acyclicity. Edge weights are sampled uniformly from $[-2, -0.5] \cup [0.5, 2]$, ensuring coefficients are bounded away from zero to exclude negligible causal effects. To ensure observations have approximately unit variance and fall within the $[-2, 2]$ range, we normalize the weight matrix by rescaling $\mathbf{W} \leftarrow \mathbf{D}^{-1/2}\mathbf{W}$ where $\mathbf{D} = \text{diag}(\mathbf{T}\mathbf{T}^\top)$ and $\mathbf{T} = (\mathbf{I} - \mathbf{W})^{-1}$ denotes the transfer matrix. To avoid varsortability (Reisach et al., 2021), we scale all variables of the generated data to unit variance.

Atomic Interventions Interventional data is generated following Pearl’s do-calculus: for an intervention $\text{do}(t)$, we remove all incoming edges to the intervened node and set its value to $c \sim \text{Unif}([0.5, 1.5])$, simulating a gene perturbation experiment where the treated genes have varying perturbation efficiencies. To condition the model on the treatment, we use a d -dimensional one-hot-encoding, where the element at the hot index contains the intervention value c .

Experiment Design We intervene on each of the 20 nodes in 1000 randomly generated DAGs to generate all 20k possible context/treatment conditions. Per treatment condition, we sample $n = 500$ pre-perturbation observations, resulting in 10M interventional vector-valued samples. Additionally, we generate 500 untreated observations per DAG, adding to a total of 10.5M samples. For MapPFN, we use a context \mathcal{C} with $K = 4$ perturbation experiments.

B.2. Synthetic Biological Prior

To generate synthetic perturbation datasets across diverse contexts, we combine a preferential attachment algorithm for sampling graphs with properties close to real GRNs (Aguirre et al., 2025) and SERGIO (Dibaeinia & Sinha, 2020) for simulating observations from these graphs using Hill functions and adding technical noise. Our goal is maximally broad but relevant prior coverage. We sample from a family of SERGIO settings validated across 15 real datasets (Dibaeinia & Sinha, 2020) and exclude technical noise configurations that do not match the 10x Chromium sequencing protocol, as we found these had the largest impact on distributional similarity.

Gene Regulatory Networks GRNs have unique properties that we want the prior to replicate. As summarized by Aguirre et al. (2025), these properties are (1) sparsity, (2) directed edges and cycles, (3) asymmetry of in- and out-degree distributions and (4) modularity. To ensure our dataset captures the diversity of GRNs, we sample the hyperparameters uniformly from ranges suggested by Aguirre et al. (2025), as summarized in Table 5.

Since SERGIO requires GRNs that are acyclic, we remove cycles by removing the edge with the smallest absolute weight in each cycle. Additionally, SERGIO requires at least one master regulator (MR), i.e. genes with no incoming edges but at least one outgoing edge. If no MRs exist after cycle removal, we select the top 5% of genes with the lowest in-degree among all genes with outgoing edges and remove all incoming edges, forcing them to become MRs.

Table 5. GRN structure parameters for the graph generator.

Symbol	Description	Range
k	Number of gene groups/modules	$\{1, 2, 3\}$
p	Sparsity term (avg. regulators per gene)	$[1.5, 3.0]$
δ_{in}	In-degree uniformity term	$[10, 300]$
δ_{out}	Out-degree uniformity term	$[1, 30]$
w	Modularity term (within-group connectivity)	$[1, 900]$

Table 6. SERGIO simulation and technical noise parameters.

Symbol	Description	Range
<i>Simulation parameters</i>		
k	Interaction strengths	$[1.0, 5.0]$
b	Master regulator production rates	$[0.5, 2.0] \cup [3.0, 5.0]$
γ	Hill function coefficients (nonlinearity)	$[1.5, 2.5]$
λ	Decay rates per gene	$[0.5, 1.0]$
ζ	Stochastic process noise scale	$[0.5, 1.5]$
<i>Technical noise parameters</i>		
μ_{outlier}	Log-normal outlier mean	$[0.8, 5.0]$
μ_{lib}	Log-normal library size mean	$[4.5, 6.0]$
σ_{lib}	Log-normal library size std	$[0.3, 0.7]$
δ	Dropout percentile	$[8.0, 8.0]$
ξ	Dropout temperature	$[45.0, 82.0]$

Simulation Given a regulatory network sampled in the previous step, we simulate single-cell expressions using SERGIO (Dibaeinia & Sinha, 2020). SERGIO models the expression level of each gene as a function of its regulators using Hill functions (Gesztelyi et al., 2012). It then models the gene interaction dynamics by solving a Stochastic Differential Equation (SDE) called chemical Langevin equation (CLE; Gillespie, 2000). Single-cell expression values are generated by applying technical noise to the steady state of this system. We sample the hyperparameters for the simulation and technical noise uniformly from the ranges summarized in Table 6. For improved simulation speed, we use a reimplementaion of SERGIO in Rust (Chatzaroulas, 2024).

Experiment Design We sample single-cell data in 6000 synthetic GRNs of 50 genes and simulate $n = 200$ single-cells expressions per treatment condition. We use a context \mathcal{C} containing $K = 8$ perturbation experiments.

B.3. Single-cell Perturbation Datasets

We obtain two single-cell perturbation datasets from `perty` (Heumos et al., 2025). Both use CRISPR knockout perturbations, matching the hard interventions modeled by SERGIO. To keep the synthetic prior grounded in a well-understood simulator validated against real gene expression data (Dibaeinia & Sinha, 2020), we restrict evaluation to datasets compatible with this intervention type. CRISPRi-based datasets, such as those in the Virtual Cell Challenge (Roohani et al., 2025), induce soft knockdowns and require extending the simulator to support partial gene suppression.

Melanoma Dataset The first dataset (Frangieh et al., 2021) contains approximately 218,000 cells measured using Perturb-CITE-seq under 248 CRISPR gene knockout perturbations. Perturbed genes were selected by their membership in an immune evasion program associated with resistance to immunotherapy. The knockout perturbations were measured in three patient-derived melanoma cell lines, comprising one untreated control, one treated with interferon- γ (IFN- γ) to put the cells into an alarmed state and a co-culture treated with tumor infiltrating lymphocytes (TIL) to simulate an immune response. For our experiments, we use the cell line treated with IFN- γ as the hold-out context.

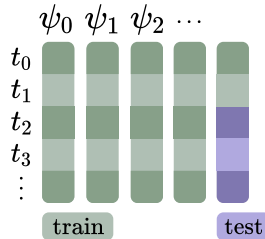


Figure 4. Data split. Each box represents a dataset $Y_{ij}^{int} \in \mathbb{R}^{N \times d}$ sampled from the SCM ψ_i under treatment t_j . Green boxes are part of the training data and purple boxes are withheld for evaluation. Following the Virtual Cell Challenge (Roohani et al., 2025), the training data includes interventional distributions from a subset of perturbations in the test context. MapPFN makes predictions only using this subset as interventional context, while all baselines are trained on the full training set.

Leukemia Dataset The second dataset (Papalexi et al., 2021) was generated using ECCITE-seq, a multimodal assay combining scRNA-seq with surface protein measurements, on the THP-1 monocytic leukemia cell line. Cells were stimulated with IFN- γ , decitabine (DAC) and TGF- β 1 to induce PD-L1 expression. CRISPR perturbations target 26 genes involved in immune checkpoint regulation. After quality control and assignment to a single perturbation, approximately 20,000 cells are available for analysis. Unlike the melanoma dataset, this dataset contains a single biological context.

Experiment Design For both datasets, we select the set of perturbed genes and fill the remaining slots to 50 genes with the top marker genes, identified by differential expression analysis between each perturbation and control using `sc.tl.rank_genes_groups`. We sample $n = 200$ i.i.d. cells per condition.

Preprocessing Following best practice for single-cell RNA sequencing preprocessing (Luecken & Theis, 2019), we first normalize the total counts per cell to be equal to the median total count across all cells, followed by a `log1p` transform

$$\tilde{\mathbf{x}} = \log_2 \left(1 + \frac{m \cdot \mathbf{x}}{\|\mathbf{x}\|_1} \right) \tag{5}$$

where $m = \text{median}_i(\|\mathbf{x}_i\|_1)$ is the median total count across all cells. We use the implementation of `sc.pp.normalize_total` and `sc.pp.log1p` provided by `scanpy` (Wolf et al., 2018).

B.4. Data Split

We split the data at the condition level, where each condition corresponds to a context-treatment pair (ψ_i, t_j) . Each pair is assigned independently to the train, validation, or test split, ensuring that the samples of a particular context/treatment condition are only contained in a single split. Half of the treatments of the holdout context are assigned to the test split, while the other half is included in the train split. Figure 4 shows a visualization of the data split. To obtain a validation set, randomly select 10% of the remaining train conditions.

C. Experimental Details

C.1. Baselines

For comparability, MapPFN and all baselines are conditioned on one-hot encoded treatments.

CPA The Compositional Perturbation Autoencoder (CPA; Lotfollahi et al., 2023) decomposes cell states into independent basal state, treatment, and covariate embeddings using a variational autoencoder. Perturbation effects are modeled as additive shifts in latent space, enabling combinatorial generalization to unseen treatment combinations.

CondOT Conditional Optimal Transport (CondOT) trains a partially input-convex neural network (PICNN; Amos et al., 2017) to learn a global conditional OT map for different treatment conditions or subpopulations (Bunne et al., 2022). We use the identity initialization, as the Gaussian initialization requires target distribution statistics that are unavailable for unseen contexts.

Meta Flow Matching Meta Flow Matching (MFM; [Atanackovic et al., 2025](#)) proposes to integrate the vector fields on the Wasserstein manifold by conditioning the flow on a learned representation of the observational distribution. With the aim of modeling interactions between individual cells, MFM separately trains a graph neural network (GNN) yielding population embeddings.

CellFlow CellFlow ([Klein et al., 2025](#)) uses flow matching to learn a transport from the source to the perturbed cell distribution. Perturbation covariates are encoded into a condition embedding that guides the flow. To handle arbitrary numbers of perturbations in a permutation-invariant manner, CellFlow employs set aggregation with multihead attention.

STATE STATE ([Adduri et al., 2025](#)) consists of a State Transition model (ST) that predicts perturbation effects on sets of cells, and an optional State Embedding model (SE) that provides pre-trained cell representations from large-scale observational data. ST uses self-attention over sets of observational cells to predict perturbed cell populations, modeling interactions between cells within each set. Since our gene sets are low-dimensional, we use the ST model on raw expression profiles.

C.2. Metrics

We measure the discrepancy between the distribution of predicted samples and the distribution of ground-truth samples. We evaluate our models in terms of distributional, correlation and ranking-based metrics.

Wasserstein Distance The entropy-regularized Wasserstein distance ([Cuturi, 2013](#)) between ground-truth samples $\mathbf{Y} \in \mathbb{R}^{n \times d}$ and predicted samples $\hat{\mathbf{Y}} \in \mathbb{R}^{m \times d}$ is computed as

$$W_2(\mathbf{Y}, \hat{\mathbf{Y}}) := \left(\min_{\mathbf{P} \in \mathcal{U}(\mathbf{Y}, \hat{\mathbf{Y}})} \sum_{i=1}^n \sum_{j=1}^m \mathbf{P}_{ij} \| \mathbf{y}_i - \hat{\mathbf{y}}_j \|_2^2 - \epsilon H(\mathbf{P}) \right)^{1/2} \quad (6)$$

where ϵ is the regularization parameter, $\mathcal{U}(\mathbf{Y}, \hat{\mathbf{Y}})$ is the set of transport matrices of shape $n \times m$ given by

$$\mathcal{U} = \left\{ \mathbf{P} \in \mathbb{R}_{\geq 0}^{n \times m} : \mathbf{P} \mathbf{1}_m = \frac{1}{n} \cdot \mathbf{1}_n \text{ and } \mathbf{P}^\top \mathbf{1}_n = \frac{1}{m} \cdot \mathbf{1}_m \right\} \quad (7)$$

and H is the entropy computed as $H(\mathbf{P}) = -\sum_{ij} \mathbf{P}_{ij} \log \mathbf{P}_{ij} - 1$. To obtain a valid distance that becomes zero if and only if the compared distributions are equal, we use the Sinkhorn divergence ([Feydy et al., 2019](#); [Genevay et al., 2018](#)) given by

$$S_2(\mathbf{Y}, \hat{\mathbf{Y}}) = W_2(\mathbf{Y}, \hat{\mathbf{Y}}) - \frac{1}{2} W_2(\mathbf{Y}, \mathbf{Y}) - \frac{1}{2} W_2(\hat{\mathbf{Y}}, \hat{\mathbf{Y}}) \quad (8)$$

We use the implementation provided by the optimal transport tools (OTT) package ([Cuturi et al., 2022](#)) with the regularization parameter $\epsilon = 0.1$.

Maximum Mean Discrepancy The squared maximum mean discrepancy (MMD; [Gretton et al., 2012](#)) between ground truth and predicted samples \mathbf{Y} and $\hat{\mathbf{Y}}$ for a conditionally positive definite kernel k is defined as

$$\text{MMD}^2(\mathbf{Y}, \hat{\mathbf{Y}}) = \mathbb{E}_{\mathbf{y}, \mathbf{y}'} [k(\mathbf{y}, \mathbf{y}')] + \mathbb{E}_{\hat{\mathbf{y}}, \hat{\mathbf{y}}'} [k(\hat{\mathbf{y}}, \hat{\mathbf{y}}')] - 2\mathbb{E}_{\mathbf{y}, \hat{\mathbf{y}}} [k(\mathbf{y}, \hat{\mathbf{y}})] \quad (9)$$

We compute the MMD for the Gaussian radial basis function (RBF) kernel

$$k_{\text{RBF}}(\mathbf{x}, \mathbf{y}) = \exp(-\gamma \| \mathbf{x} - \mathbf{y} \|_2^2) \quad (10)$$

and report the mean over multiple length scales $\gamma \in \{10, 1, 0.1, 0.01, 0.001\}$.

Root Mean Squared Error We follow [Wu et al. \(2025b\)](#) in computing the root mean squared error (RMSE)

$$\text{RMSE}(\mathbf{Y}, \hat{\mathbf{Y}}) = \sqrt{\frac{1}{n} \sum_i (\hat{\mu}_i - \mu_i)^2} \quad (11)$$

between the mean of the predicted and ground-truth post-perturbation distributions $\boldsymbol{\mu} = \mathbb{E}[\mathbf{y}^{\text{int}}]$ and $\hat{\boldsymbol{\mu}} = \mathbb{E}[\hat{\mathbf{y}}^{\text{int}}]$.

Table 7. Hyperparameter search ranges for each method.

Method	Hyperparameter	Search Range
MapPFN	Classifier-free guidance weight	{1.0, 1.5, 2.0, 2.5, 3.0}
CPA	Following the tuning protocol of PerturBench (Wu et al., 2025b).	
CondOT	Hidden dimensions	{64, 128, 256}
	Hidden layers	{2, 3, 4}
MFM	k-nearest neighbors	{0, 10, 50, 100}
	GNN embedding dimensions	{64, 128, 256}
CellFlow	Following the reference notebook (Klein et al., 2025).	
STATE	Following the reference notebook (Adduri et al., 2025).	

Perturbation Discrimination Score To evaluate whether model predictions are distinguishable across perturbations, we adopt the perturbation discrimination score (PDS) from Wu et al. (2025b). Let $\mu_i = \mathbb{E}[\mathbf{y}_i^{\text{int}}]$ and $\hat{\mu}_i = \mathbb{E}[\hat{\mathbf{y}}_i^{\text{int}}]$ denote the mean observed and predicted expression for perturbation i , respectively. The PDS measures, for each perturbation i , what fraction of other observations μ_j are closer to $\hat{\mu}_i$ than the matched observation μ_i :

$$\text{Rank}_{\text{avg}}^\top = \frac{1}{p} \sum_{i=1}^p \text{Rank}^\top(\hat{\mu}_i), \quad \text{Rank}^\top(\hat{\mu}_i) = \frac{1}{p-1} \sum_{\substack{1 \leq j \leq p \\ j \neq i}} \mathbb{I}(d(\hat{\mu}_i, \mu_j) \leq d(\hat{\mu}_i, \mu_i)) \quad (12)$$

where p is the number of perturbations and d is the Euclidean distance. This metric ranges from 0 (perfect) to 1 (worst), with 0.5 corresponding to random predictions. The PDS is particularly sensitive to mode collapse, as a model generating similar predictions for all perturbations will have many ground-truth observations closer than the matched one.

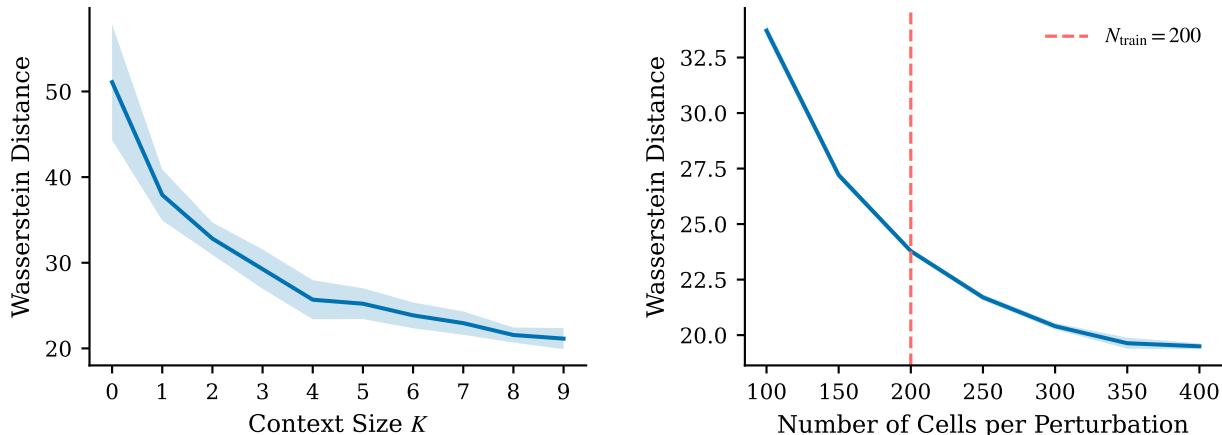
Area Under the Precision Recall Curve To evaluate whether model predictions reliably imply identification of differentially expressed genes (DEGs), we adopt the AUPRC metric from Zhu et al. (2025). For a given perturbation, ground-truth DEGs are identified using a per-gene Wilcoxon rank-sum test comparing single-cell expression values before and after intervention, under the null hypothesis of identical distributions (Wilcoxon, 1945). Benjamini-Hochberg (Benjamini & Hochberg, 2000) correction is applied across genes, and DEGs are defined by jointly thresholding on effect size and statistical certainty, using the absolute \log_2 fold-change ($\tau_l = 0.2$) and the negative \log_{10} p-value ($\tau_p = 2$).

$$Z_g = \mathbb{I}(\tilde{p}_g > \tau_p \wedge |\tilde{l}_g| > \tau_l) \quad (13)$$

where $\tilde{p}_g = -\log_{10}(p_g)$ and $\tilde{l}_g = \log_2(\tilde{\mu}_g^{\text{int}}/\tilde{\mu}_g^{\text{obs}})$ denote the negative log p-value and log fold-change for gene g , respectively. For in silico predictions, we compute a ranking score $R_g = |\tilde{l}_g| \cdot \mathbb{I}(\tilde{p}_g > \tau_p)$ that combines the magnitude of predicted expression change with statistical significance. By varying a threshold r on this score, we generate a family of classifiers $\hat{Z}_g(r) = \mathbb{I}(R_g > r)$ and construct precision-recall curves against the ground-truth labels Z_g . The AUPRC summarizes model performance, with the baseline AUPRC given by $\pi = (\text{number of DEGs})/(\text{total genes})$, corresponding to random ranking. As an additional baseline for gene knockout perturbations, we consider a predictor that assigns a positive score only to the perturbed gene. Differential expression analysis was performed using `scanpy.tl.rank_genes_groups` (Wolf et al., 2018).

C.3. Hyperparameters

By default, we use the hyperparameters recommended by the authors of each baseline. We follow the Optuna-based tuning protocol of PerturBench (Wu et al., 2025b) for CPA, perform a small grid search for CondOT and MFM, and use the published reference configurations for STATE (Adduri et al., 2025) and CellFlow (Klein et al., 2025). For MapPFN, we only grid-search the classifier-free guidance weight. The searched hyperparameters are summarized in Table 7.



(a) **Context size scaling.** Wasserstein distance on the melanoma dataset for varying numbers of perturbation experiments in the context set \mathcal{C} . Performance improves monotonically with context size $K = |\mathcal{C}|$, with diminishing returns beyond four experiments. Shaded regions indicate standard deviation over three seeds.

(b) **Cell set scaling.** Wasserstein distance on the melanoma dataset for varying numbers of cells per perturbation in context. Performance improves beyond the training configuration (dashed line). A model that does not perform in-context learning would be expected to plateau. Shaded regions indicate standard deviation over ten resampling seeds.

Figure 5. MapPFN improves with more data at inference time. Both the number of perturbation experiments in context and the number of cells per perturbation improve prediction quality, demonstrating that MapPFN adapts to the available data via in-context learning.

C.4. Implementation

We use JAX (Bradbury et al., 2018) to implement our experiments. Our model is implemented using equinox (Kidger & Garcia, 2021) and diffrax (Kidger, 2022) for ODE solving. We also make use of Optimal Transport Tools (OTT) (Cuturi et al., 2022) to compute the Sinkhorn distance. We use hydra-zen (Soklaski et al., 2022) to configure our experiments. For single-cell data processing, we build upon the scverse ecosystem, including anndata (Virshup et al., 2024), scanpy (Wolf et al., 2018) and pertpy (Heumos et al., 2025).

We run our experiments on a high-performance cluster, using a single NVIDIA A100 or H100 GPU with 80 GB of VRAM for training. For the linear SCM dataset, each experiment ran for 2-8h depending on the method and configuration. Pre-training MapPFN on synthetic single-cell data took approximately 10-36h, depending on the setting and corresponding context size.

D. Additional Results

D.1. Test-time Scaling

To evaluate how the performance of MapPFN scales with the amount of interventional experiments provided in context, we measure the Wasserstein distance for varying context sizes $K = |\mathcal{C}|$. As shown in Figure 5a, test performance improves monotonically as additional perturbation experiments are provided in context, with diminishing returns beyond four interventional experiments. This indicates that conditioning on interventional data enables the model to learn perturbation-specific mappings that are not accessible to approaches conditioning only on the treatment identifier or the observational distribution.

To evaluate how performance scales with the number of cells per perturbation, we vary the number of cells at inference time. As shown in Figure 5b, performance improves with more cells, without plateauing at the number of cells seen during training (dashed line). This suggests that MapPFN can leverage more data by adapting at inference time via in-context learning.

D.2. Prior Coverage

Figure 6 compares the expression and log fold change distributions of the synthetic prior with both real datasets. Overall, the synthetic prior covers the range of expression values and perturbation effects observed in both downstream datasets. For the melanoma dataset (Frangieh et al., 2021), the distributional shapes align well, which is reflected in strong zero-shot

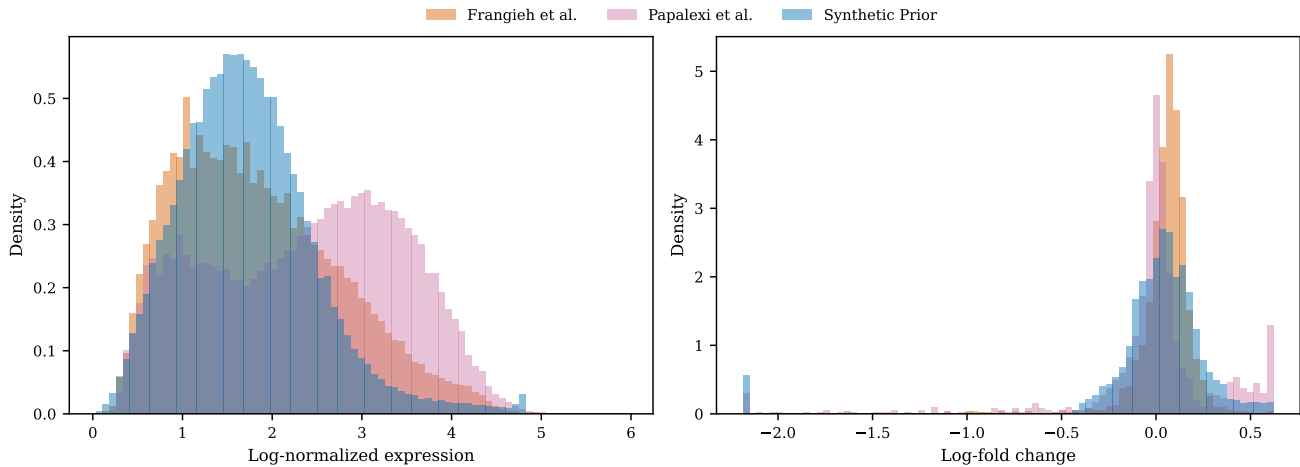


Figure 6. Coverage of the synthetic prior over real single-cell data distributions. Expression and log fold change distributions for the synthetic biological prior, the melanoma (Frangieh et al., 2021) and leukemia (Papalexi et al., 2021) datasets. The prior covers the range of expression values and perturbation effects observed in real data.

performance. For the leukemia dataset (Papalexi et al., 2021), the expression distribution is bimodal, which may explain the reduced zero-shot performance on this dataset. Fine-tuning achieves strong performance on both datasets (Table 3), showing that MapPFN can compensate for distributional differences between synthetic and real data.